Journal of Materials Processing Technology 226 (2015) 106–114

Contents lists available at ScienceDirect

Journal of Materials Processing Technology

journal homepage: www.elsevier.com/locate/jmatprotec

# Microstructure formation and precipitation in laser welding of microalloyed C–Mn steel

Xiao-Nan Wang[a,d], Chang-Jun Chen[b], Hai-Sheng Wang[a,c], Shun-Hu Zhang[a,*], Min Zhang[b], Xia Luo[a]

[a] School of Iron and Steel, Soochow University, Suzhou 215021, PR China
[b] Laser Processing Research Center, School of Mechanical and Electrical Engineering, Soochow University, Suzhou 215021, PR China
[c] School of Materials Science & Engineering, Anhui University of Technology, Ma'ansha 243002, PR China
[d] Jiangsu Provincial Key Laboratory for Science and Technology of Photon Manufacturing, Jiangsu University, Zhenjiang 212013, PR China

ARTICLE INFO

*Article history:*
Received 20 November 2014
Received in revised form 10 July 2015
Accepted 11 July 2015
Available online 18 July 2015

*Keywords:*
Laser welding
Steel
Precipitation
Phase transformation
Hardness measurement
Martensite

ABSTRACT

A 4-kW fiber laser was adopted to weld nano-scale precipitate-strengthened C–Mn steel (NPS steel). Only martensite was found in the fusion zone (FZ), fusion line and coarse-grained heat-affected zone (CGHAZ). The heat-affected zone (HAZ) consisted of both ferrite and martenite/austenite island (M/A island), which were found in both the fine-grained heat-affected zone (FGHAZ) and the mix-grained heat-affected zone (MGHAZ). In the FZ, original niobium titanium carbonitride and niobium titanium carbide precipitates were completely re-dissolved in the re-heating process, and only niobium titanium carbonitride re-precipitated in the subsequent cooling process. The original precipitates coarsened in heat-affected zone (HAZ) like Ostwald ripening phenomenon. Micro-hardness and yield strength of the FZ and the HAZ were higher than those in the base material (BM). Compared with the BM, the strengthening mechanism of the FZ and the CGHAZ were transformation strengthening and grain-refinement strengthening; precipitate strengthening. Transformation strengthening was the primary and important strengthening mechanism in the FGHAZ and the MGHAZ.



## 1. Introduction

Wang et al. (2013) had recently developed a nano-scale precipitate-strengthened C–Mn steel (NPS steel), which had been successfully applied in heavy duty truck frames and carriages. NPS steel application could reduce 20% weight of the truck. The NPS steel showed a fine microstructure with a large number of dispersed (Nb,Ti)C precipitates with diameters less than 15 nm, resulting in a high tensile strength above 700 MPa. Despite of its excellent mechanical properties and formability, the microstructures of the NPS steel welding joint could be varied with the process of conventional $CO_2$ gas-shielded welding, which led to the low strength and unstable performance of the joints. Fatigue fracture was therefore prone to occur at the welded joint due to low strength (Wang et al., 2012).

The welding process was a metallurgical process that involves the processes of solidification, phase transformations and carbide precipitation or dissolution (Zhao et al., 2009). Hsu et al. (2012) applied autogenously gas tungsten arc welding on nano-precipitated high strength steels and studied the effect of heat input (1.2–3.0 kJ/mm) and cooling rate (15–30 °C/s) on the formation of nano re-precipitates in the weld metal (i.e., the solidified fusion zone). They concluded that the re-precipitation of nano TiC could only be observed at high heat input (3.0 kJ/mm) because higher the heat input, slower the cooling rate and more time for the occurrence of precipitation. Moon and Lee (2009) reported that both compressive and tensile deformations improved the coarsening rate of (Ti,Nb)CN precipitates in the coarse-grained heat-affected zone (CGHAZ) of Ti + Nb microalloyed steel and precipitation of (Ti,Nb)CN could be promoted by deformation.

Laser welding had been applied on joining various steels and proven to be effective in enhancing the joint quality (Katayama, 2013), due to its high energy density, narrow heat affected zone, low distortion and large depth to width ratio, etc., Němeček et al. (2012) investigated the differences between laser and arc welding of TRIP 900 steel tubes and martensitic sheets DOCOL 1200. They concluded that the tensile strength of conventional welds was significantly lower than that of the base material. Laser welds exhibited comparable strength when compared with the base material. As for ANSI 304 stainless steel, Zhang et al. (2013) demon-

* Corresponding author. Fax: +86 512 67165621.
*E-mail address:* 28044105@qq.com (S.-H. Zhang).

http://dx.doi.org/10.1016/j.jmatprotec.2015.07.010
0924-0136/

**Table 1**
Chemical composition of the NPS steel (elements in wt.%).

| C | Mn | Si | Nb | Ti | P | S | Fe |
|---|---|---|---|---|---|---|---|
| 0.08–0.12 | 1.7–2.0 | 0.2–0.3 | 0.02–0.05 | 0.08–0.15 | < 0.005 | < 0.005 | Balance |

**Table 2**
Mechanical properties of the NPS steel.

| Yield strength/MPa | Tensile strength/MPa | Elongation/% | Cold bending 180° |
|---|---|---|---|
| 625 | 720 | 22.0 | Qualified |

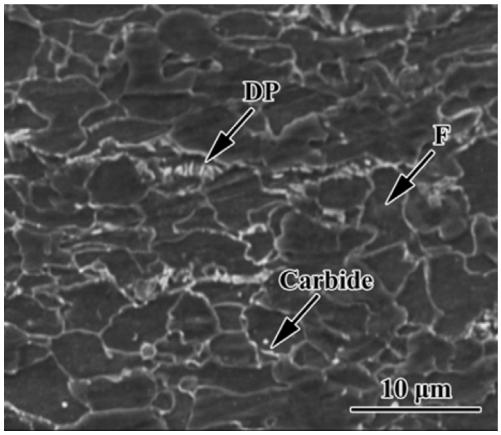


**Fig. 1.** SEM image of unwelded specimens (F—ferrite, DP—degenerated pearlite).

strated that the fiber-laser welded joints showed the lowest tensile residual stress, the highest micro-hardness and tensile strength when compared with $CO_2$ and Nd:YAG laser welded ones.

No research had been applied laser welding on NPS steel to improve the welded joint quality. In this study, the NPS steel specimens were welded by fiber-laser welding under different heating and cooling conditions. The evolution of the microstructure, nano-scale precipitate and hardness of the NPS steel-welded joint were systematically investigated. Based on the results, change of the strengthening mechanism could be released.

## 2. Materials and methods

### 2.1. Materials

The NPS steel with a tensile strength of 700 MPa grade was used for the following laser welding procedures. Table 1 depicts the chemical composition of the NPS steel. The hot-rolled NPS steel strips with a thickness of 6.2 mm were completed on a 1780 mm hot rolling production line. Table 2 shows the mechanical properties of the NPS steel strips, which indicated a good balance between strength and toughness.

Fig. 1 shows scanning electron microscopy (SEM) image of the as-received substrate. The microstructure was mainly comprised of ferrite (F) grains (dark grey), a small amount of degenerated pearlite (DP) (white), and some carbide along the ferrite grain boundaries. The average diameter of ferrite grains ranged from 4 μm to 6 μm.

### 2.2. Methods

The laser welding of untreated square shaped (200 mm × 50 mm × 6.2 mm) NPS steel plates was carried out using a continuous-wave fiber laser (IPG YLS-4000) system with a maximum power of 4 kW, and the laser welding head was mounted on a robotic arm (KUKA KR30HA). The spot diameter of the laser beam was 0.86 mm with a focal length of 300 mm. The ultra-high argon (Ar) was selected as the shielding gas with a flow rate of 1.0 $m^3$/h. The laser welding process parameters used in this study were shown in Table 3.

**Table 3**
Laser welding process parameters in the experiments.

| Laser power ($P$)/kW | Welding speed ($v$)/m/min | Defocusing distance ($\Delta f$)/mm |
|---|---|---|
| 3.5 | 0.78 | −1 |
| 3.5 | 1.00 | −1 |
| 3.5 | 1.20 | −1 |

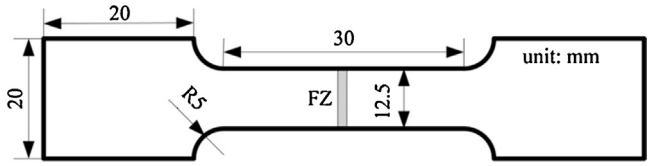


**Fig. 2.** Schematic diagram of tensile test specimens design.

After the fiber laser welding, the specimens were cut cross-sectionally by electro-discharge machining. The cross-section specimens were polished and then etched with 4% nital solution before they were examined under the Nanguang Z00M1020 stereomicroscope, FEI Quanta 600 scanning electron microscope (SEM) and Hitachi S-4700 field-emission scanning electron microscope (SEM). To study the size, morphology and distribution of precipitates, carbon extraction replicas of the NPS steel laser welded joint were observed using a Tecnai $G^2$ F20 transmission electron microscope at 200 kV. The micro-hardness of the welded joints was evaluated using a HXD-1000TMC/LCD micro-hardness tester with a Vickers diamond indenter under a load of 1.961 N with a loading time of 10 s at room temperature of 25 °C. The transverse tests were conducted using a universal tensile-testing machine (RGM-4100) operated at a crosshead speed of 3 mm/min, and the tensile fracture was observed using SEM. Fig. 2 shows the design of specimens for tensile testing. FZ was located in the middle of the specimen.

## 3. Results and discussion

Fig. 3 illustrates the surface appearance and cross-sections of the welded joints manufactured at different welding speeds ($v$) under a laser power ($P$) of 3.5 kW and at a defocusing distance ($\Delta f$) of −1 mm. It could be seen from Fig. 3a that the penetration depth ($h$) was 5.35 mm when the welding speed was 1.20 m/min. When the welding speed decreased to 1.00 m/min, most of the area was fully penetrated (Fig. 3c). The area enclosed in the white dashed frame had a penetration depth of 5.99 mm (Fig. 3d). The discontinuous welded seam as indicated by the black frame implied that the full depth penetration was not stable when the welding speed was 1.00 m/min. When the welding speed reduced to 0.78 m/min, full depth penetration and continuous welded seam could be observed as shown in Fig. 3e and f. Therefore, laser power of 3.5 kW, welding speed 0.78 m/min and defocusing distance −1 mm were used to produce laser welded joints for the following microstructure and properties analysis and discussion.

### 3.1. Microstructure evolution

The overall microstructure around the welded seam was observed using stereomicroscope. Fig. 4 depicts a transverse cross section of the laser-welded joint. The welded joint consisted of fusion zone (FZ), heat-affected zone (HAZ) and base metal (BM). As shown in Fig. 4, HAZ contained three regions, namely coarse-grained heat-affected zone (CGHAZ), fine-grained heat-affected zone (FGHAZ) and mix-grained heat-affected zone (MGHAZ). The